

Article

Indentation-Free Resistance Spot Welding of SUS301L Stainless Steel

Yutong Liu ¹, Yuming Xie ^{1,2,*}, Xiuwen Sun ¹, Licheng Sun ¹, Naijie Wang ², Xiaotian Ma ², Xiangchen Meng ^{1,2} 
and Yongxian Huang ^{1,2,*} 

¹ State Key Laboratory of Precision Welding and Joining of Materials and Structures, Harbin Institute of Technology, Harbin 150001, China; 2021110889@stu.hit.edu.cn (Y.L.); 23b909132@stu.hit.edu.cn (X.S.); sunlicheng@sjtu.edu.cn (L.S.); mengxch@hit.edu.cn (X.M.)

² Zhengzhou Research Institute, Harbin Institute of Technology, Zhengzhou 450046, China; wangnaijie@hit.edu.cn (N.W.); maxiaotian@hit.edu.cn (X.M.)

* Correspondence: ymxie@hit.edu.cn (Y.X.); yxhuang@hit.edu.cn (Y.H.)

Abstract: Paint-free bodywork has become an attractive alternative for rail vehicles, in the direction of easy maintainability and low manufacturing costs. However, conventional resistance spot welding inevitably leaves indentation marks to detrimentally reduce the optical homogeneity of the paint-free bodywork. In light of this, indentation-free resistance spot welding is proposed for joining SUS301L stainless steel sheets in order to achieve superior surficial integrity. A tiny SUS301L steel ball with a diameter of 1.5 mm was chosen as the intermediate filler between two steel sheets to avoid the formation of surficial indentation. The influence of welding current and welding time on the mechanical properties of joints was studied. The optimal parameters of the mechanical properties were obtained when the welding current was 8.0 kA, the welding time was 150 ms, the electrode pressure was 0.35 MPa, and the electrodes were cylindrical planar electrodes, which was determined by comparing the tensile shear test results. The surficial indentation depth was less than 1% of the plate thickness, and no observable indentations were seen on the surface of the optimized welding spots.

Keywords: stainless steel; resistance spot welding; indentation-free welding; mechanical properties



Citation: Liu, Y.; Xie, Y.; Sun, X.; Sun, L.; Wang, N.; Ma, X.; Meng, X.; Huang, Y. Indentation-Free Resistance Spot Welding of SUS301L Stainless Steel. *Metals* **2024**, *14*, 1178. <https://doi.org/10.3390/met14101178>

Academic Editor: António Bastos Pereira

Received: 30 August 2024

Revised: 7 October 2024

Accepted: 16 October 2024

Published: 16 October 2024



Copyright: © 2024 by the authors. Licensee MDPI, Basel, Switzerland. This article is an open access article distributed under the terms and conditions of the Creative Commons Attribution (CC BY) license (<https://creativecommons.org/licenses/by/4.0/>).

1. Introduction

Paint-free bodywork offers advantages, such as environmental protection, easy maintainability, and low manufacturing costs, making it an appealing alternative for rail vehicles [1]. SUS301L is currently the most commonly used material for rail vehicles and automobile bodies due to its attractive appearance, paint-free properties, anti-corrosion capabilities, and lightweight nature [2,3]. One of the significant technical challenges in achieving paint-free bodywork is indentation at the weld joints [4].

Resistance spot welding is extensively utilized in the welding of steel sheet structures for automobiles and rail vehicles because of its brief welding duration, uncomplicated process, and high level of automation [5–7]. More than 90% of assembly work in a car body is completed by resistance spot welding at present [8–10], and there are 2000 to 5000 spots made by resistance spot welding on each car in rail vehicles [11,12]. While ensuring the safety and reliability of joints, it is particularly important to study the surface quality of the spot-welded joints of paint-free stainless steel rail vehicles [13–15]. An obvious indentation will always be left on the surface of the thin sheet due to the technical characteristics of resistance spot welding, which not only affects the aesthetics of the body but also reduces the corrosion resistance of the joints [16,17]. The realization of indentation-free resistance spot welding of SUS301L stainless steel is of great significance for the production of paint-free rail vehicles.

The welding current, welding time, and electrode pressure are three key process parameters that affect the joint quality of the resistance spot welding process [18–20]. Sreehari et al. [21] found, concerning the indentation levels, that welding time has a lesser influence when compared to welding current and electrode force. Gong et al. [22] found that increasing compressive residual stress can improve the brittle fracture resistance and corrosion resistance of metal materials. Han et al. [23] explored the effect of the indentation on the sizing of the spot weld nugget. The results show that the existence of an indentation may result in under-sizing of the nugget. Pouranvari et al. [24] studied the mechanical performance of dissimilar resistance spot welding between DP600 and AISI 1008 low-carbon steels, concluding that increases in welding current and welding time result in increases in electrode indentation depth. Rajesh et al. [25] used the Taguchi approach to optimize the control parameters of the dual pulse resistance welding of 2 mm ASTM A240 stainless steel sheets. The findings indicate that the magnitude of the second pulse current is the most important component that influences indentation in dual pulse resistance spot welding. Qi et al. [26] designed a magnetically assisted resistance spot welding (MA-RSW) device for unilateral surface indentation of the traditional stainless steel RSW joint. The welding penetration rate was reduced by using single-sided MA-RSW at the permanent rate, thus the thermal influence on the base metal surface was reduced, and the surface indentation depth was reduced by more than 45% compared with the traditional process. Xia et al. [27] designed a robotic servo gun and an accompanying displacement monitoring system. Joint quality can be measured online and the welding parameters can be adjusted through this system to reduce the impact of surface indentation. These studies show the factors and control methods that affect the indentation of resistance spot welding, but they cannot achieve complete indentation-free spot welding.

In this paper, we propose a novel indentation-free resistance spot welding process. A tiny steel ball was chosen as the intermediate filler to avoid the formation of surficial indentation. The surface indentation, nugget morphology, microstructure, and macroscopic mechanical properties of the joint were investigated in detail.

2. Materials and Methods

Respectively, 0.6-mm-thick and 1.5-mm-thick SUS301L stainless steel sheets (Hebei Jingche Railway Vehicle Equipment Co., Ltd., Baoding, China) were used as upper sheets and lower sheets. The thin sheets were more easily deformed and released stress, so they were used to reduce the deformation of thick sheets. The intermediate filler was a SUS301L stainless steel ball with a diameter of 1.5 mm. The composition and mechanical properties of SUS301L are listed in Tables 1 and 2. Both the upper and lower electrodes used in spot welding are cylindrical planar electrodes with a diameter of 20 mm. Electrodes were connected to a water-cooling device for rapid cooling.

Table 1. Composition of SUS301L stainless steel (wt.%).

Element	C	Si	N	Mn	P	S	Ni	Cr	Fe
Mass fraction	0.02	0.50	0.10	1.0	0.03	0.006	7.00	17.00	Bal.

Table 2. Mechanical properties of SUS301L stainless steel.

Material	Ultimate Tensile Strength (MPa)	Yield Strength (MPa)	Elongation (%)
SUS301L	930	685	20

A resistance spot welding process for thin and thick plates was developed to reduce surface indentation. The process flow is illustrated in Figure 1. A tiny steel ball was initially welded onto the thin plate using a small welding current, welding time, and electrode pressure, followed by welding between the two sheets. Choosing the right size ball was

important for the welding process. The large diameter of the ball caused a large gap between the two plates, resulting in low joint strength. The steel ball with a very small diameter melted instantly and was not able to work. In this study, we chose steel balls with a diameter of 1.5 mm.

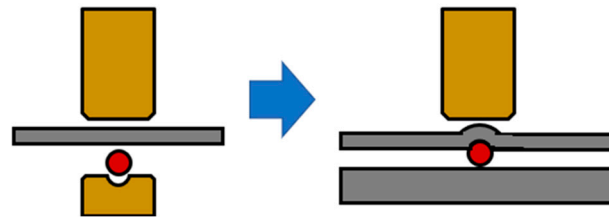


Figure 1. Process of indentation-free resistance spot welding.

Figure 2 shows the principle of the indentation-free resistance spot welding process. This method achieved low current density (J) at the surface of the base metal in contact with the electrode, while concentrating current at the middle layer of the steel ball. According to Ampere's law and resistance law, the resistance heat generated by current is related to resistivity (ρ), cross-sectional area (S), current density, and time (t). The calculation formula for resistance heat generated by current flowing through a conductor per unit thickness is as follows:

$$Q = \rho J^2 S t$$

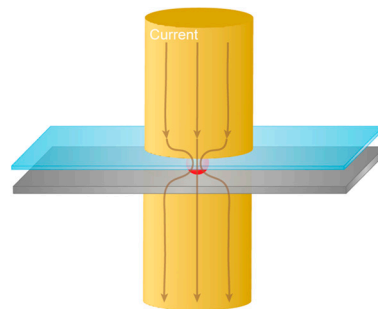


Figure 2. Principle of indentation-free resistance spot welding.

Large-diameter electrodes were used to increase the contact area between the electrode and the steel plate. The position of the steel ball has a much smaller cross-sectional area than other sites. A high current density in the middle layer of the steel ball generated significant resistance heat, causing the steel ball to melt and form a spot welding nugget. The resistance heat generated by low current density on the surface of the welded base metal in contact with the electrode was minimal. The surface indentation, ablation, and welding deformation were reduced in this way.

A copper electrode with a pit was utilized to position the ball during spot welding of the ball and sheet. The welding current was set at 1.5 kA, with a welding time of 150 ms, and an electrode pressure of 0.10 MPa.

Welding spatter was prone to occur due to the high current density at the steel ball when welding two sheets. To solve this problem, a preheating input of 2 kA welding current, 100 ms welding time, and electrode pressure of 0.35 MPa was applied before welding two sheets. According to preliminary trials, the electrode pressure was set at 0.35 MPa. Welding current and welding time were selected for optimization. We set the welding current at 7.0 kA, 7.5 kA, 8.0 kA, and 8.5 kA and the welding time at 120 ms, 150 ms, 180 ms, and 210 ms.

The metallographic and tensile shear test samples were prepared perpendicularly to the cross-sections of the resistance spot-welding joints by electric wire cutting. The metallographic samples were ground, polished, and etched with a mixture of hydrofluoric acid and nitric acid for 7 min. The cross-sectional morphology, microstructure, and

surface indentation of each zone of the sample were observed using a VHX-1000E optical microscope (Keyence, Osaka, Japan). A KC-X1000 laser confocal microscope (Kathmatic, Nanjing, China) was used to obtain the contour of the joint surface, and a straight line on the indentation was selected to measure the indentation contour.

The tensile shear sample size is 50 mm \times 15 mm, as shown in Figure 3. The tensile shear test was carried out on an electronic universal material test machine at ambient temperature with a tensile speed of 2 mm/min. The specimens were grasped with shims that were equal in thickness to the sheets. The typical fracture was observed and analyzed using a Zeiss Merlin Compact scanning electron microscope.

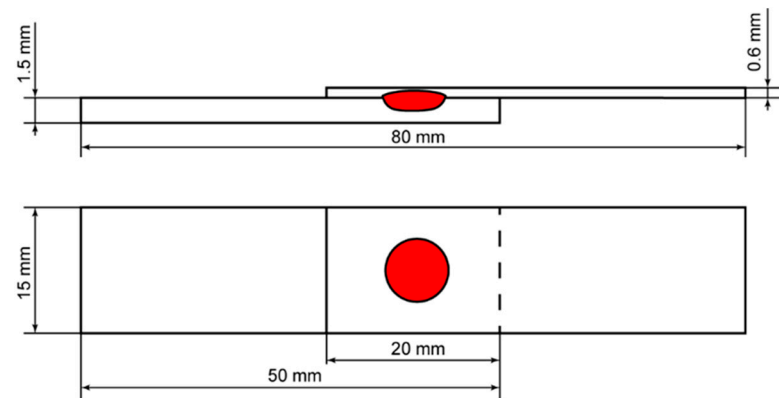


Figure 3. Dimensions of tensile shear test specimens.

3. Results and Discussion

The macroscopic morphology of welding between a 1.5 mm diameter ball and a 0.6 mm thick steel sheet is shown in Figure 4. The steel ball was deformed under the action of welding heat input and electrode pressure, but the outline remained circular. The pitted part of the steel ball did not produce large resistance heat, so it retained the original shape, and played a role in welding between the two sheets.



Figure 4. Appearance of 1.5 mm diameter steel ball welded onto 0.6 mm thick sheet.

The macroscopic morphology of several groups of indentation-free resistance spot welding process joints is shown in Figure 5. The surface indentation of the joint was minimal, and there were no ablation marks or color changes on the surface, resulting in a regular circular shape. There was almost no deformation on the side surface of the thick plate. Variations in welding parameters had little impact on the surface indentation and tablation marks of the joint within a certain range. This phenomenon was attributed to the larger contact area between the planar electrode and the thick plate side compared to that between the steel ball and steel plate, leading to relatively low current density and heat input on the thick surface of the plate. As a result, the surface indentation, welding deformation, and ablation marks were small. Changes in welding parameters did not greatly affect the surface morphology of spot-welded joints.

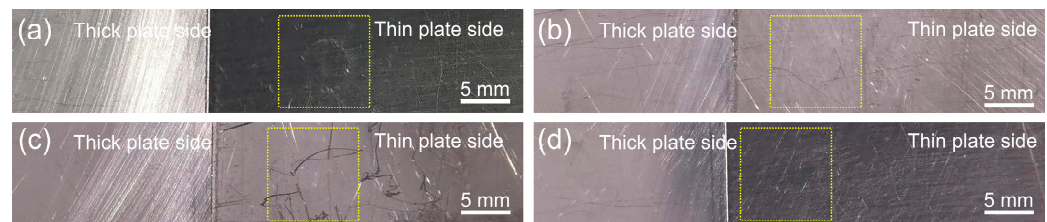


Figure 5. Surface morphology of spot-welded joints: (a) 7.0 kA, 150 ms, 0.35 MPa, (b) 7.5 kA, 150 ms, 0.35 MPa, (c) 8.0 kA, 150 ms, 0.35 MPa and (d) 8.0 kA, 180 ms, 0.35 MPa.

Figure 6 shows the nugget geometry of the indentation-free resistance spot-welding joint under different welding parameters, as observed through an optical microscope. The nugget shape of the joint showed a basin shape with a wide upper and narrow lower, which is because the resistance heat generated by the intermediate filler under the action of current constraint was larger than that on the thick plate side. However, because the intermediate filler was also affected by the current density, the welding parameters will greatly impact the spot-welding nugget. In this study, the penetration rate is expressed as the percentage of the thickness of the nugget on the side of the thick plate in proportion to the thickness of the thick plate. The nugget diameter increased from 4.80 mm at 7.5 kA to 5.18 mm at 8.0 kA as the welding current increased, and the penetration rate also increased from 47% to 58%. Welding spatter occurred when the welding current was increased to 8.5 kA. The nugget diameter was 4.07 mm and the penetration rate was 57% at this time, which is smaller than that at 8.0 kA, and the nugget size at the joint interface and the sheet side was also small. This is because the welding spatter caused the heat at the joint interface to be lost as the liquid metal flew away, further leading to insufficient heat input and poor fusion at the joint interface. It is necessary to avoid poor fusion and spatter to ensure the load-bearing capacity of the spot-welded joint. The effect of welding time on nugget morphology is similar to that of welding current. The nugget diameter and penetration rate increased from 4.53 mm and 56% at 120 ms to 5.18 mm and 58% at 150 ms with the increase in welding time.

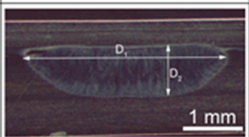
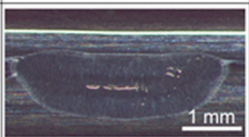
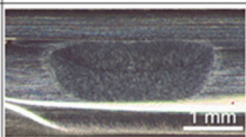
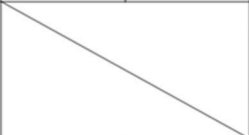
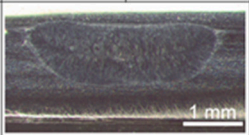
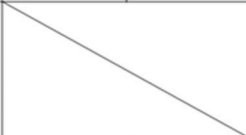
		Welding Current , kA					
		7.5		8		8.5	
Welding Time, ms	150						
		$D_1=4.80$ mm	$D_2=1.23$ mm	$D_1=5.18$ mm	$D_2=1.52$ mm	$D_1=4.07$ mm	$D_2=1.50$ mm
	120						
		$D_1=4.53$ mm		$D_2=1.47$ mm			

Figure 6. Nugget morphologies of resistance spot weld joint.

Figure 7 shows the microstructure of the resistance spot weld joints (8.0 kA, 120 ms, 0.35 MPa). Typical zones of the joint were the nugget zone and the heat-affected zone. The width of the heat-affected zone was small and was mainly composed of the coarse austenite grains formed by recrystallization, due to the rapid cooling effect of the water in the electrode [28]. This area was considered the weak point of the joint. The nugget zone consisted of columnar austenite grains growing from the thin plate and thick plate to the nugget center, because the temperature gradually decreased from the nugget to both sides.

However, the molten steel ball was extruded towards both sides of the nugget to form an extrusion zone, as shown in Figure 8c. This zone was also classified as a heat-affected zone. Two different forms of the joint were found at the joint interface between the nugget and the thin plate (shown by the yellow line in Figure 7), corresponding to Figure 8a,b, respectively.

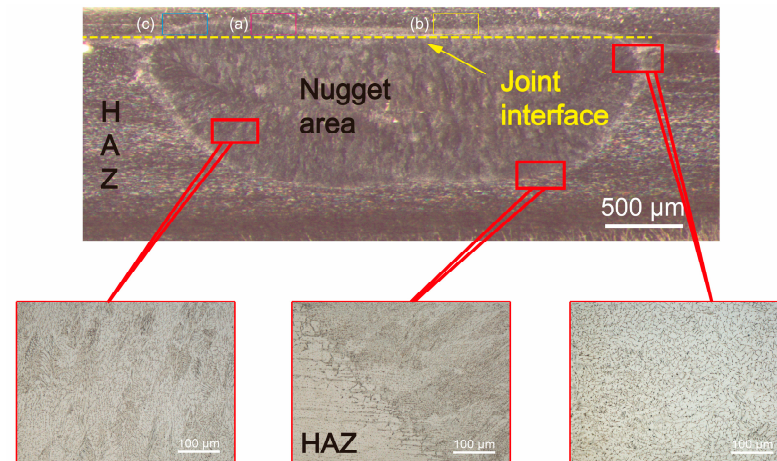


Figure 7. Microstructure of resistance spot-welding joint: (a) sampling position of Figure 8a, (b) sampling position of Figure 8b, and (c) sampling position of Figure 8c.

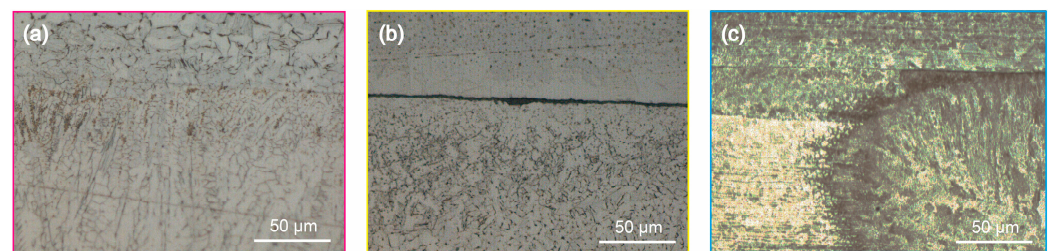


Figure 8. Interfaces of the welded joints: (a) no obvious interface, (b) distinct interface with cracks, and (c) interface with extruded steel ball.

Figure 8a shows the transition form of the normal resistance spot-welding joint from the nugget zone to the heat-affected zone. This transition is characterized by a shift from columnar crystals to coarse equiaxed austenite grains, with no obvious joint interface. As shown in Figure 8b, the area with an obvious joint interface was located in the middle of the nugget, at the position of the pre-welded steel ball of the thin plate. There was an obvious joint interface in this area, which accounted for about one-third of the diameter of the nugget, which seriously affected the mechanical properties of spot-welded joints. The area can be considered as incomplete fusion at the joint interface. According to the location and joint of the zone shown in Figure 8b, the formation of this zone was related to the process of pre-welding steel balls for the sheet. A small welding current and welding time were adopted in the process of welding the sheet and steel balls. Although this can maintain the shape of the steel ball and make it connect with the sheet to a certain extent, the joint was not strong. There was an obvious joint interface between the plate and the steel ball. In the process of base metal welding, the contact resistance between the steel ball and the thick plate generated a large amount of resistance heat at the joint of the steel ball and the thick plate, causing this area to form a good fusion. However, the contact resistance between the steel ball and the thin plate disappeared in the step of welding two sheets. This resulted in insufficient heat input at the position, causing the original joint state to remain unchanged and leading to poor fusion in the interface area. The fracture position of the joint was located at the joint interface between the thin plate and the nugget in the subsequent fracture analysis, which agreed with the above analysis of the cause of the poor fusion.

A set of tests was designed to study the changing trend of the maximum tensile shear of the joint with the welding current. The specific process parameters are shown in Table 3. An increase in welding current led to the highest maximum tensile shear and nugget diameter. However, welding spatter occurred at 8.5 kA, resulting in a decrease in maximum tensile shear.

Table 3. Welding current and welding time test parameters.

Samples	Welding Current	Welding Time	The Highest Value of Tensile Shear Force	Welding Spatter (Yes/No)
1	7.0 kA	150 ms	6027 N	N
2	7.5 kA	150 ms	6052 N	N
3	8.0 kA	150 ms	6414 N	N
4	8.5 kA	150 ms	5530 N	Y
5	8.0 kA	120 ms	6403 N	N
6	8.0 kA	180 ms	6489 N	N
7	8.0 kA	210 ms	5810N	Y

The variation trend in the maximum tensile shear of spot-welded joints was studied under the condition that only the power on time was changed on this basis. The maximum tensile shear force increased with the increase in welding time, but the increase was small. The maximum tensile shear plummeted when the welding time was 210 ms due to the welding spatter.

Figure 9a,b shows the maximum tensile shear force of specimens at various welding currents and the load–displacement curve of the four groups of corresponding parameters. Figure 9c,d shows the variation trend in the maximum tensile shear force with welding time and the load–displacement curves of the four groups of corresponding parameters. The optimal parameters of the mechanical properties were obtained when the welding current was 8.0 kA, the welding time was 150 ms and the electrode pressure was 0.35 MPa. To predict the tensile shear force of resistance spot-welded thin steel sheets, Majlinger et al. [29] recommended a formula based on the materials' tensile strength and the sheet thickness:

$$TSF = -10.10 + 0.0088 \cdot R_m + 15.80 \cdot t \text{ (kN)}$$

In this formula, *TSF* is the predicted shear tensile strength of the optimized joints, *R_m* is the tensile strength of the steel in MPa and *t* is the sheet thickness in mm. The maximum tensile shear force obtained under the optimal parameters is predicted to be 7.564 kN according to this formula. The experimental values were close to the predicted values.

We speculated that the optimal parameters obtained may be mainly influenced by the size of the nugget. With the increase in welding current and welding time, the nugget size increases, and the effective bonding area of the joint also increases. Excessive heat input led to welding spatter and large welding residual stress when the welding current or welding time was too large, and the mechanical properties decreased therefore [30,31].

Figure 10 shows the macro fracture morphology of samples 1–4. The macro fracture interface shown in the figure was the fracture morphology of the thick plate side. The fracture mode of the tensile shear specimen of samples 1, 2, and 4 was the interface fracture mode. The fracture occurred at the position between the thin plate and the nugget (incomplete fusion zone). For the tensile shear specimen of sample 3, the fracture mode of the tension-shear specimen was button fracture mode. The fracture position was in the heat-affected zone on the thin side, and the fracture interface did not pass through the nugget but broke along the heat-affected zone on the sheet side. It is generally considered that the button fracture mode of the joint is better than the interface fracture mode [32]. The extrusion zone of sample 3 (as shown in Figure 10c) and the thin plate side were first separated and formed a smooth fracture interface, indicating that its strength was low.

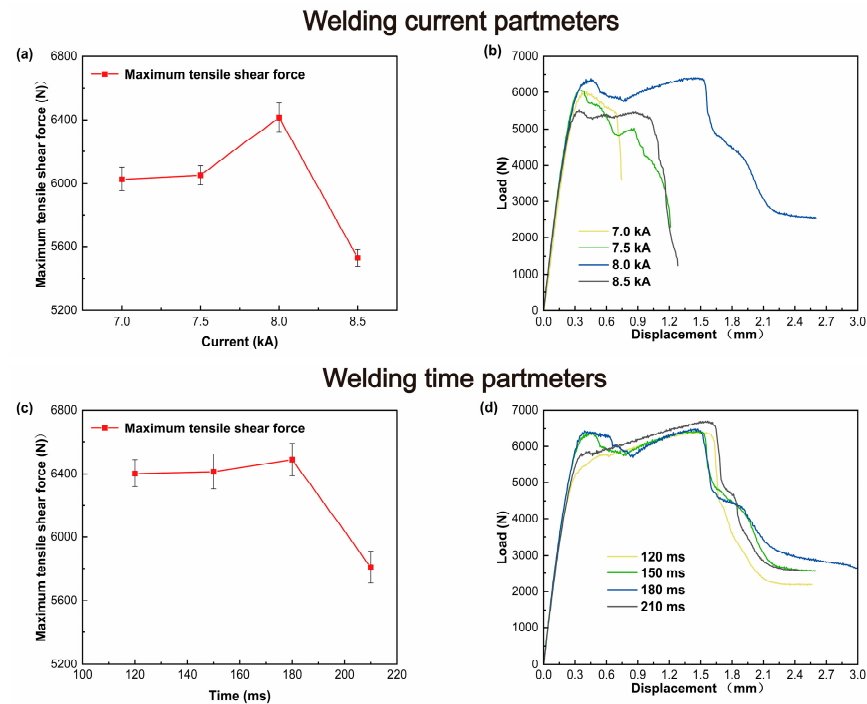


Figure 9. Tensile shear curve with different parameters: (a) tensile shear force curve with different welding currents, (b) load–displacement curve, (c) tensile shear force curve with different welding time, and (d) load–displacement curve.

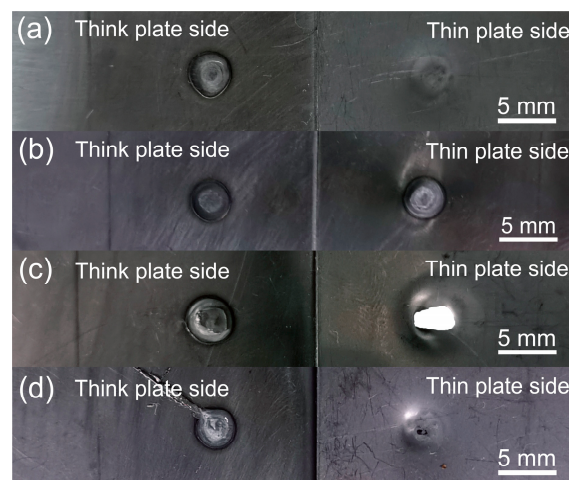


Figure 10. Fracture surface morphology of RSW joint: (a) 7.0 kA, 150 ms, 0.35 MPa, (b) 7.5 kA, 150 ms, 0.35 MPa, (c) 8.0 kA, 150 ms, 0.35 MPa, and (d) 8.5 kA, 150 ms, 0.35 MPa.

The fracture interface morphology and fracture position of the spot-welded joint are shown in Figure 11. The maximum tensile shear of the button fracture mode samples was larger than that of the interface fracture mode samples. This was consistent with the results of the maximum tensile shear curve shown in Figure 6. The reason was related to the incomplete fusion at the joint of the thin plate and the nugget. The incomplete fusion reduced the bonding strength at the joint interface of the nugget and the thin plate side, so that the interface fracture mode occurred.

Figure 12a,b shows the surface indentation morphology of the RSW joint obtained under the optimal parameters of mechanical properties (8.0 kA, 150 ms and 0.35 MPa). The indentation was shallow and presented a regular circle. Figure 12c shows the indentation contour of the red line segment in Figure 12b. The height difference between the indentation on the joint surface and the base material was small. The maximum indentation height

difference was about 25 μm . The maximum indentation depth was about 1% of the plate thickness for the thick plate side with a thickness of 1.5 mm. It can be considered that the surface of the spot welding joint had no indentation under this set of parameters.

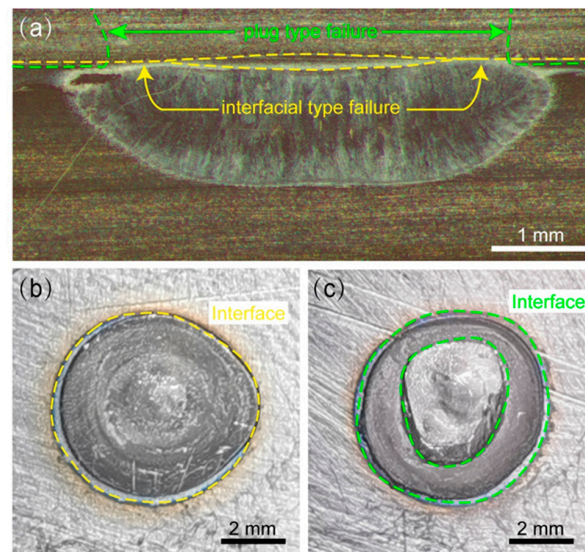


Figure 11. Fracture interface morphologies and fracture locations: (a) nugget morphology of the joint, 8.0 kA, 180 ms, 0.35 MPa, (b) macroscopic fracture interface of interfacial fracture mode, 7.0 kA, 150 ms, 0.35 MPa, and (c) macroscopic fracture interface of button fracture mode, 8.0 kA, 150 ms, 0.35 MPa.

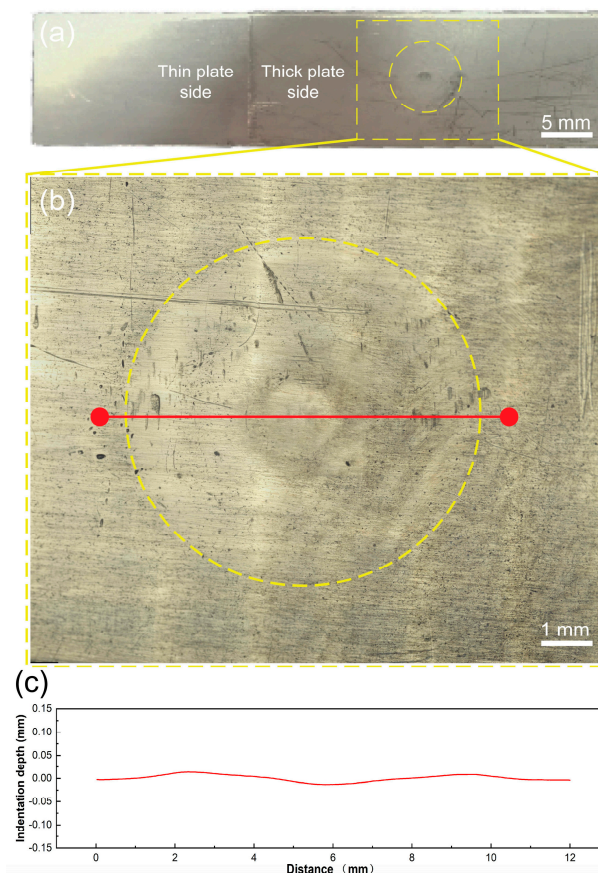


Figure 12. Surface morphologies of the joint. (a) Macroscopic indentation on the side surface of the thick plate, (b) the thick plate side indentation under an ultra-deep microscope, and (c) indentation depth of the red line joint surface.

4. Conclusions

This paper proposed a novel resistance spot welding process through the intermediate layer of steel balls to confine the current and obtain an indentation-free surface on one side of the spot-welding joint. The process changed the current density of different parts, resulting in high current density at the nugget. The resistance heat is concentrated in the intermediate filler. The surface of the plate had a small welding heat input, leading to minimal deformation, indentation, and ablation marks. The highest value of tensile shear force increased with increasing welding current or welding time. Welding spatter occurred when the welding current or welding time was too large, which decreased the highest value of tensile shear force. The microstructure of this joint was similar to that of traditional resistance spot-welding joints. The maximum tensile shear force reached 6414 N when the welding current was 8.0 kA, the welding time was 150 ms, and the electrode pressure was 0.35 MPa, by using cylindrical planar electrodes. The surface indentation depth of the joint under this set of parameters was about 1% of the plate thickness at this time, and almost no indentations could be achieved.

Author Contributions: Conceptualization, Y.L. and Y.X.; methodology, Y.L. and X.S.; validation, L.S.; formal analysis Y.X. and X.M. (Xiaotian Ma); investigation N.W. and X.M. (Xiaotian Ma); writing—original draft preparation Y.L.; writing—reviewing and editing, X.M. (Xiangchen Meng), Y.H. and Y.X. All authors have read and agreed to the published version of the manuscript.

Funding: This work was jointly supported by the National Natural Science Foundation of China (Nos. 52305345, 52175301, 52205350).

Data Availability Statement: The data presented in this study are available on request from the corresponding author. The data are not publicly available due to privacy restrictions.

Conflicts of Interest: The authors declare no conflicts of interest.

References

1. Xu, W.; Zhang, B.; Deng, Y.; Wang, Z.; Jiang, Q.; Yang, L.; Zhang, J. Corrosion of rail tracks and their protection. *Corros. Rev.* **2021**, *39*, 1–13. [\[CrossRef\]](#)
2. Fu, Z.H.; Li, T.; Shan, M.L.; Gou, G.Q.; Zhu, Z.Y.; Ma, C.P.; Gao, W.; Hu, Y.C. Hydrogen atoms on the SCC behavior of SUS301L-MT stainless steel laser-arc hybrid welded joints. *Corros. Sci.* **2019**, *148*, 272–280. [\[CrossRef\]](#)
3. Li, J.; Luo, X.; Ma, G.; Wang, J.; Pan, J.; Ruan, Q. The effect of cold rolled reduction ratios on grain boundary character and mechanical properties of the SUS301L austenitic stainless steel. *Mater. Res. Express* **2019**, *6*, 126587. [\[CrossRef\]](#)
4. Kalyankar, V.D.; Chudasama, G.P. Influence of electrode tip diameter on metallurgical and mechanical aspects of spot welded duplex stainless steel. *High Temp. Mater. Process.* **2020**, *39*, 317–327. [\[CrossRef\]](#)
5. Martín, Ó.; Tiedra, P.D.; López, M.; San-Juan, M.; García, C.; Martín, F.; Blanco, Y. Quality prediction of resistance spot welding joints of 304 austenitic stainless steel. *Mater. Des.* **2009**, *30*, 68–77. [\[CrossRef\]](#)
6. Feng, Q.B.; Li, Y.B.; Carlson, B.E.; Lai, X.M. Study of resistance spot weldability of a new stainless steel. *Sci. Technol. Weld. Join.* **2019**, *24*, 101–111. [\[CrossRef\]](#)
7. Banga, H.K.; Kalra, P.; Kumar, R.; Singh, S.; Pruncu, C.I. Optimization of the cycle time of robotics resistance spot welding for automotive applications. *J. Adv. Manuf. Process.* **2021**, *3*, e10084. [\[CrossRef\]](#)
8. Pouranvari, M.; Alizadeh-Sh, M.; Marashi, S.P.H. Welding metallurgy of stainless steels during resistance spot welding part I: Fusion zone. *Sci. Technol. Weld. Join.* **2015**, *20*, 502–511. [\[CrossRef\]](#)
9. Akkas, N. Welding time effect on tensile-shear loading in resistance spot welding of SPA-H weathering steel sheets used in railway vehicles. *Acta Phys. Pol. A* **2017**, *131*, 52–54. [\[CrossRef\]](#)
10. Zhou, K.; Yao, P. Overview of recent advances of process analysis and quality control in resistance spot welding. *Mech. Syst. Signal Process.* **2019**, *124*, 170–198. [\[CrossRef\]](#)
11. Pouranvari, M.; Marashi, S.P.H. Critical review of automotive steels spot welding: Process, structure and properties. *Sci. Technol. Weld. Join.* **2013**, *18*, 361–403. [\[CrossRef\]](#)
12. Al-Mukhtar, A. Review of Resistance Spot Welding Sheets: Processes and Failure Mode. *Adv. Eng. Forum* **2016**, *17*, 31–57. [\[CrossRef\]](#)
13. Jou, M. Real time monitoring weld quality of resistance spot welding for the fabrication of sheet metal assemblies. *J. Mater. Process. Technol.* **2003**, *132*, 102–113. [\[CrossRef\]](#)
14. Wang, H.X.; Wang, C.S.; Shi, C.Y.; Xiao, J.F. The Investigation of Partial Penetration Lap Laser Welding Applied on Stainless Steel Railway Vehicles. *Adv. Mater. Res.* **2010**, *97*, 3832–3835. [\[CrossRef\]](#)

15. Cheon, J.Y.; Vijayan, V.; Murgun, S.; Do Park, Y.; Kim, J.H.; Yu, J.Y.; Ji, C. Optimization of pulsed current in resistance spot welding of Zn-coated hot-stamped boron steels. *J. Mech. Sci. Technol.* **2019**, *33*, 1615–1621. [\[CrossRef\]](#)
16. He, L.; DiGiovanni, C.; Han, X.; Mehling, C.; Wintjes, E.; Biro, E.; Zhou, N.Y. Suppression of liquid metal embrittlement in resistance spot welding of TRIP steel. *Sci. Technol. Weld. Join.* **2019**, *24*, 579–586. [\[CrossRef\]](#)
17. Song, S.; Shojaei, M.; Midawi, A.R.H.; Sherepenko, O.; Ghassemi-Armaki, H.; Biro, E. Influence of expulsion and heat extraction resulting from changes to electrode force on liquid metal embrittlement during resistance spot welding. *J. Mater. Res. Technol.* **2023**, *23*, 1458–1470. [\[CrossRef\]](#)
18. Fukumoto, S.; Fujiwara, K.; Toji, S.; Yamamoto, A. Small-scale resistance spot welding of austenitic stainless steels. *Mater. Sci. Eng. A Struct.* **2008**, *492*, 243–249. [\[CrossRef\]](#)
19. Jagadeesha, T. Experimental studies in weld nugget strength of resistance spot-welded 316L austenitic stainless steel sheet. *Int. J. Adv. Manuf. Technol.* **2017**, *93*, 505–513. [\[CrossRef\]](#)
20. Biradar, A.K.; Dabade, B.M. Optimization of resistance spot welding process parameters in dissimilar joint of MS and ASS 304 sheets. *Mater. Today Proc.* **2020**, *26*, 1284–1288. [\[CrossRef\]](#)
21. Sreehari, M.; Bhaskar, G.B. Experimental investigations on resistance spot welding for producing indentation free joints on AISI 409M grade stainless steels. *Mater. Res. Express* **2019**, *6*, 46527. [\[CrossRef\]](#)
22. Gong, Z.; Zhang, T.; Chen, Y.; Lu, J.; Ding, X.; Zhang, S.; Lan, M.; Shen, Y.; Wang, S. Effect of laser shock peening on stress corrosion cracking of TC4/2A14 dissimilar metal friction stir welding joints. *J. Mater. Res. Technol.* **2024**, *30*, 1716–1725. [\[CrossRef\]](#)
23. Han, X.; Wu, W.; Xiao, L. Effect of Spot Weld Indentation on Spot Weld Nugget Characterization. In Proceedings of the 2018 IEEE International Ultrasonics Symposium (IUS), Kobe, Japan, 22–25 October 2018. [\[CrossRef\]](#)
24. Pouranvari, M. Influence of welding parameters on peak load and energy absorption of dissimilar resistance spot welds of DP600 and AISI 1008 steels. *Can. Metall. Q.* **2011**, *50*, 381–388. [\[CrossRef\]](#)
25. Rajesh, D.; Chandran, V.; Lenin, N.; Subramanian, A.; Deva, M.; Balamurugan, P. Optimization of dual pulse resistance welding parameters for ASTM A240 stainless steel sheets: A multi-objective approach. *Interactions* **2024**, *245*, 140. [\[CrossRef\]](#)
26. Qi, L.; Li, F.; Zhang, Q.; Xu, Y.; Han, X.; Li, Y. Improvement of single-sided resistance spot welding of austenitic stainless steel using radial magnetic field. *ASME J. Manuf. Sci. Eng.* **2021**, *143*, 031004. [\[CrossRef\]](#)
27. Xia, Y.-J.; Su, Z.-W.; Lou, M.; Li, Y.-B.; Carlson, B.E. Online Precision Measurement of Weld Indentation in Resistance Spot Welding Using Servo Gun. *IEEE Trans. Instrum. Meas.* **2020**, *69*, 4465–4475. [\[CrossRef\]](#)
28. Xie, J.; Chen, Y.; Wang, H.; Zhang, T.; Zheng, M.; Wang, S.; Yin, L.; Shen, J.; Oliveira, J.P. Phase transformation mechanisms of NiTi shape memory alloy during electromagnetic pulse welding of Al/NiTi dissimilar joints. *Mater. Sci. Eng. A* **2024**, *893*, 146119. [\[CrossRef\]](#)
29. Majlinger, K.; Katula, L.T.; Varbai, B. Prediction of the Shear Tension Strength of Resistance Spot Welded Thin Steel Sheets from High- to Ultrahigh Strength Range. *Period. Polytech. Mech.* **2022**, *66*, 67–82. [\[CrossRef\]](#)
30. Chen, L.; Zhang, Y.; Xue, X.; Wang, B.; Yang, J.; Zhang, Z.; Tyrer, N.; Barber, G.C. Investigation on shearing strength of resistance spot-welded joints of dissimilar steel plates with varying welding current and time. *J. Mater. Res. Technol.* **2022**, *16*, 1021–1028. [\[CrossRef\]](#)
31. Shawon, M.R.A.; Gulshan, F.; Kurny, A.S.W. Effect of Welding Current on the Structure and Properties of Resistance Spot Welded Dissimilar (Austenitic Stainless Steel and Low Carbon Steel) Metal Joints. *J. Inst. Eng. Ser. D* **2015**, *96*, 29–36. [\[CrossRef\]](#)
32. Pouranvari, M.; Marashi, S.P.H. Failure Behavior of Three-Steel Sheets Resistance Spot Welds: Effect of Joint Design. *J. Mater. Eng. Perform.* **2012**, *21*, 1669–1675. [\[CrossRef\]](#)

Disclaimer/Publisher’s Note: The statements, opinions and data contained in all publications are solely those of the individual author(s) and contributor(s) and not of MDPI and/or the editor(s). MDPI and/or the editor(s) disclaim responsibility for any injury to people or property resulting from any ideas, methods, instructions or products referred to in the content.